Journal of Power Sources 223 (2013) 341–348

Contents lists available at SciVerse ScienceDirect

Journal of Power Sources

journal homepage: www.elsevier.com/locate/jpowsour

Exsolution of nickel nanoparticles at the surface of a conducting titanate as potential hydrogen electrode material for solid oxide electrochemical cells

Charline Arrivé [a,b], Thibaud Delahaye [a,*], Olivier Joubert [b], Gilles Gauthier [a,1]

[a] CEA, LITEN, 17 rue des Martyrs, F-38054 Grenoble cedex 9, France
[b] Institut des Matériaux jean Rouxel (IMN), Université de Nantes, CNRS, 2 Rue de la Houssinière, BP 32229, 44322 Nantes cedex 3, France

HIGHLIGHTS

- New titanate, $La_{0.5}Sr_{0.5}Ti_{0.75}Ni_{0.25}O_3$, was proposed as hydrogen electrode for SOCs.
- Ni exsolution was studied via reduction *in situ* at 800 °C and at higher temperature.
- Both reduction and pre-reduction lead to precipitation of Ni nanoparticles.
- After pre-reduction conductivity was improved probably due to the formation of Ti^{3+}.
- Polarization resistance was measured equal to 0.56 Ω cm^2 at 800 °C in H_2/H_2O (3%).

ARTICLE INFO

Article history:
Received 18 June 2012
Received in revised form
11 September 2012
Accepted 17 September 2012
Available online 23 September 2012

Keywords:
SOFC
SOEC
Hydrogen electrode
Perovskite
Titanate
Exsolution

ABSTRACT

A new $La_{0.5}Sr_{0.5}Ti_{0.75}Ni_{0.25}O_3$ (LSTN25) titanate was proposed as a hydrogen electrode for Solid Oxide Cells (SOCs) with electrochemical performance given by Ni nanoparticles exsoluted at the surface of a conducting oxide. As only *in-situ* reduction at 800 °C has been proposed in literature to perform Ni exsolution, the reduction at higher temperature of the LSTN25 compound was also considered in this work. The high-temperature treatment led to the precipitation of Ni nanoparticles evidenced by TEM observation and to an improved electrical conductivity that may be due to the formation of a sufficiently high concentration of Ti^{3+}. Electrochemical study of symmetrical cells tested in H_2/H_2O (97/3) showed a promising performance, with a polarization resistance of 0.55 Ω cm^2 at 800 °C and 0.46 Ω cm^2 after a thermal treatment in air that simulates the air electrode sintering.

© 2012 Elsevier B.V. All rights reserved.

1. Introduction

In the field of highly efficient and fuel-flexible Solid Oxide Cells (SOFCs or SOECs), finding hydrogen electrode materials remains a scientific challenge. These compounds must have electrochemical kinetics comparable to conventional Ni-based cermets, but with reduced aging, higher robustness with respect to redox cycling, and eventually higher tolerance to sulfides and coking (in the case of SOFCs fed with realistic hydrocarbon fuels and having low or even null steam to carbon ratios). The ideal electrode material would be a monophasic compound, preferably a Mixed Ionic and Electronic Conductor (MIEC) that would present a good electrocatalytic activity for the following half-reactions:

$$H_2 + O^{2-} \rightleftarrows H_2O + 2e^- \quad (1)$$

$$C_nH_{2n+2} + (3n+1)O^{2-} \rightleftarrows nCO_2 + (n+1)H_2O + (6n+2)e^- \quad (2)$$

In this context, two material families were primarily considered as replacements for cermets, with remarkable success: doped chromites and titanates such as $La_xSr_{1-x}CrO_3$ (LSC) or $La_xSr_{1-x}TiO_3$ (LST), both presenting perovskite (or derived) structures particularly stable in reducing conditions [1–6]. But despite their good electrical properties, these materials present low electro-catalytic activities. To solve this problem without falling into the conventional cermet case, which requires percolation of both metallic and

* Corresponding author. DEN/DTEC/SDTC/LEMA, CEA/Marcoule – Bât. 166 – Atalante, BP 17171 – 30207 Bagnols sur Cèze cedex, France. Tel.: +33 4 66 79 65 42; fax: +33 4 66 79 16 49.
E-mail address: thibaud.delahaye@cea.fr (T. Delahaye).
[1] Professor at the Universidad Industrial de Santander, Escuela de Ingeniería Química, Bucaramanga, Colombia.

0378-7753/$ – see front matter © 2012 Elsevier B.V. All rights reserved.
http://dx.doi.org/10.1016/j.jpowsour.2012.09.062

ceramic networks, small quantities of very active nanoparticles, *e.g.*, Ni or Ru, can be added to the electrode. This new "cermet" is generally obtained by impregnation of a pre-sintered conducting electrode with a metallic salt or a nanopowder suspension [7–10]. Although this kind of process has been widely used in the field of reforming catalysis, applied to SOCs it can sometimes give rise to a non-homogeneous distribution of metallic particles. Moreover, grain coarsening could also occur if other high temperature thermal treatments are required in the cell preparation process or cell testing procedure. Finally, this method requires a multi-step impregnation/thermal treatment and is difficult to implement on the industrial scale, especially for large cells.

An alternative method was proposed, wherein electrocatalyst elements initially dissolved in the perovskite structure in their oxidized state are reduced *in situ*, resulting in the precipitation of metal nanoparticles at the surface of oxide grains. This new route to obtain a cermet with a non-percolating metallic phase is called exsolution or "solid phase crystallization", and is well-known in reforming catalysis [11].

In this field, it was shown that catalysts prepared by exsolution were less sensitive to coking due to the finely-dispersed nickel nanoparticles [12]. In addition, the strong basicity of alkaline earth or rare earth oxides was reported to reduce the carbon deposition. It favors CO_2 adsorption and thus shifts the Boudouard reaction equilibrium towards CO ($2CO \rightleftarrows CO_2 + C$). Several groups have reported that catalysts derived from perovskite $LaNiO_3$ or Ruddlesden–Popper La_2NiO_4 can present a significant resistance to coking. This could be due to synergistic effects of Ni and La sites, where carbon species on Ni sites could be removed by oxygen species brought by $La_2O_2CO_3$ [13–16], with a favorable effect.

The need for better control of the catalytic activity and easier processing (no extra steps in cell fabrication) recently led to adapting the exsolution concept to hydrogen electrode materials [17–19]. Thus, in Ru- or Ni-substituted LSC, it was shown that the polarization resistance decreased during the first 100 h of cell operation due to the progressive nucleation of metal nanoclusters. To the same end, Ni-substituted LST was proposed as a new hydrogen electrode material [20]. When prepared under reducing atmosphere, LST compounds are known to have higher n-type electronic conductivities than chromites. Based on the aforementioned results, $La_{0.5}Sr_{0.5}Ti_{0.75}Ni_{0.25}O_{3-\delta}$ was synthesized and the influence of exsolution conditions (*i.e.*, the temperature of the reducing treatment) on perovskite structure and electrical and electrochemical performance was evaluated.

2. Experimental

The $La_{0.5}Sr_{0.5}Ti_{0.75}Ni_{0.25}O_{3-\delta}$ (LSTN25) compound was synthesized using a nitrate–citrate gel technique which is a variant of the Pechini method. La_2O_3 (Rhodia, 99.9%), $SrCO_3$ (Alfa Aesar, 99.99%), nickel acetate hydrate $(C_2H_3O_2)_2Ni\cdot 4H_2O$ (Alfa Aesar, >99%) and titanium isopropoxide $Ti(OCH(CH_3)_2)_4$ (Alfa Aesar, 99.995%) were used as metal precursors. La_2O_3 was weighed after dehydration and decarbonation at 1000 °C for 10 h, and $SrCO_3$ was weighed after dehydration at 400 °C for 10 h. Titanium isopropoxide, $Ti(OCH(CH_3)_2)_4$, was diluted in a mixture of ethylene glycol and citric acid to reduce the risk of precipitation during synthesis. The as-obtained solution of Ti(IV), as well as the solid nickel acetate tetrahydrate, were assayed by thermogravimetric analysis. The as-obtained precursors were added in stoichiometric proportions to a solution of nitric acid HNO_3 (65 wt%) and citric acid (Alfa Aesar, 99.5%) with an excess of complexing agent (citric acid/cation ratio = 3:1) to prevent cation precipitation.

During the concentration process, the precursor solution was neutralized to a pH of 8 by an ammonia solution (NH_4OH 28 vol%), a step that promotes the formation of a polymer network without cation precipitation. The as-formed gel was dried in an oven at 150 °C and then pyrolyzed until autocombustion occurred. The resulted very fine powder was manually ground and treated at 600 °C for 3 h (ramping of 5 °C min^{-1}) to remove most of organic matter. After homogenization, the powder was submitted to an ultimate thermal treatment at 1200 °C for 3 h in order to crystallize the expected phase. Longer thermal treatments at higher temperatures (*e.g.*, at 1300 °C for 12 h in air) allowed a better crystallization, useful for structural determination. Powder X-Ray Diffraction (XRD) patterns were obtained using a Brüker "D8 Advance" powder diffractometer operating in Bragg-Brentano reflection geometry with a Cu $K\alpha_{1,2}$ radiation (Ni filter for Kβ in front of the detector). The experimental data were refined by the Rietveld method using the FullProf 2k program and its graphical interface WinPLOTR [21].

The specific surface area of the different powders was measured by the Brunauer–Emmett–Teller (BET) method applied to N_2 adsorption and desorption at 69 K (BECKMANN COULTER sorptometer – SA 3100™ Series). Before analysis, the sample was outgassed for 3 h at 573 K. The particle size distribution was determined by ultrasonic dispersion of the powders in ethanol using a Malvern Mastersizer S laser granulometer. Dilatometry measurements were carried out by means of a Setaram DHT 2050K system on pellets that were previously pressed at 180 MPa.

The reduction behavior of the compound was investigated via thermogravimetric analysis (Setaram TGA 92) performed in Ar/H_2 (98/2) at up to 1500 °C (rate of 2 K min^{-1}), after a cleaning step from room temperature to 600 °C (rate of 10 K min^{-1}) in air to remove adsorbed species, such as water and carbonates. Based on this measurement, the LSTN25 powder was then reduced in an Ar/H_2 (98/2) flow (15 L h^{-1}) at various temperatures from 800 to 1300 °C and analyzed by XRD.

Transmission Electron Microscopy (TEM) study was carried out with a Hitachi H9000Nar electron microscope, operating at 300 kV with a Scherzer resolution of 1.8 Å. A small amount of powder was dispersed in ethanol using an ultrasonic probe. A drop of the resulting suspension was deposited on carbon-coated TEM grids.

LSTN powder was uniaxially pressed into pellets (1.5 mm thick and 10 mm in diameter) and sintered in air at 1400 °C for 5 h. Thin pellets with over 90% of the theoretical density (d_{th} = 5.85 g cm^{-3}, based on the refined lattice parameters) were obtained and cut into bars (~2 mm^2 cross-section and 8–10 mm in length). To study the influence of reduction on total conductivity, some bars were reduced under an Ar/H_2 (98/2) flow (15 L h^{-1}) at various temperatures. Total conductivity was measured by the 4-point probe DC method on dense bars. Au paste was painted on and then sintered at 750 °C for 15 min for electrical contacts. Measurements were performed in air, Ar/H_2 (98/2) and wet Ar/H_2 (98/2) (pH_2O ~ 0.025 atm) from 450 to 800 °C. A systematic correction of the total conductivity of LSTN25 samples was applied to take into account the real density of the sample using an empirical equation also used by Fu *et al.* [6]:

$$\sigma_{corr} = \frac{\sigma_{meas}}{2(C/100 - 0.5)} \quad (3)$$

where σ_{corr} is the corrected electrical conductivity, σ_{meas} is the measured apparent conductivity and C the compacity or relative density (%).

Symmetrical cells were tested to assess the electrochemical behavior of LSTN25. Dense 8YSZ (8 mol% Yttria-Stabilized Zirconia) electrolytes (∅ = 16 mm, ~100 μm thick) were obtained from a Tosoh TZ-8Y powder by tape casting then subsequent sintering at 1550 °C – 3 h. A screen-printable ink was prepared by mixing 60 wt% of LSTN25 powder and 40 wt% of an ethyl cellulose–terpineol

medium. A thin YDC (Yttria Doped Ceria) interlayer (~5 μm) was added at the 8YSZ//LSTN25 interface as a bonding layer to increase the cohesion between the dense electrolyte and porous electrode. In addition, this layer can act as a barrier layer to prevent chemical reactions and the formation of resistive phases such as $La_2Zr_2O_7$. The electrodes (∅ = 10 mm) were then deposited onto both sides of the 8YSZ substrates in 3 layers (~15 μm), then sintered in air at 1200 °C for 3 h. Two NiO layers were then deposited onto the electrodes (~10 μm). They were reduced during the pre-reduction treatment at 1200 °C for 2 h under an Ar/H_2 (98/2) flow (15 L h^{-1}) providing current collection layers of Ni with a thickness of 7–10 μm. The electrode polarization resistances were determined by Electrochemical Impedance Spectroscopy (EIS) in a two-electrode configuration using a Solartron 1260 gain phase analyzer working in a potentiostatic mode without polarization offset. The measurements were carried out at 800 °C in wet H_2 (pH_2O ~ 0.025 atm), applying an AC voltage amplitude of 30 mV in the frequency range from 10^6 to 10^{-2} Hz.

3. Results and discussion

3.1. Powder characterization

The material's powder XRD patterns after thermal treatments at 1200 °C for 3 h or 1300 °C for 12 h in air confirmed the single perovskite phase formation for the $La_{0.5}Sr_{0.5}Ti_{0.75}Ni_{0.25}O_{3-\delta}$ composition, where δ is the oxygen deficiency. A first indexing of the powder XRD pattern was performed using both Dicvol04 [22] and Checkcell [23] software programs. Successive comparisons of the more realistic solutions for perovskite-type compounds allow identification of an orthorhombic distortion with approximated cell dimensions 5.528 × 5.560 × 7.810 Å^3 (*i.e.*, a $\sqrt{2}a_p \times \sqrt{2}a_p \times 2a_p$ unit cell, where a_p is the parameter of the corresponding cubic perovskite). The most appropriate space group given by Checkcell is *Imma* (S.G. No. 74). Using such a structural description, a Le Bail Whole Pattern Fitting followed by a Rietveld refinement was carried out, giving a good agreement between the recorded and calculated patterns and a final Bragg factor (R_{Bragg}) of 4.56% ($\chi^2 = 1.09$). The observed, calculated and difference patterns, as well the calculated reflections, are plotted in Fig. 1, and the corresponding results of the refinement are summarized in Table 1. LSTN25 can be considered as a solid solution between two extreme compounds, both perovskite-type: cubic $SrTiO_3$ (S.G. P*m*-3*m*, No. 221) and $LaTi_{0.5}Ni_{0.5}O_3$ (LTN) presenting a distorted orthorhombic structure (S.G. *Pbnm*, No. 62) with an unit cell of size $\sqrt{2}a_p \times \sqrt{2}a_p \times 2a_p$ [24]. The XRD pattern is close to that of the parent compound, LTN. Nevertheless, the LSTN25 XRD pattern presents less peaks than its LTN parent, with the systematic absence of the (*hkl*) reflections with $h + k + l = 2n + 1$. Its structure is thus more symmetrical, corresponding to an I-centered lattice. The *Imma* space group, identified by systematic indexing of XRD patterns, can be described in the Glazer notation by a two-tilt system ($a^-a^-c^0$), whereas the LTN *Pbnm* space group corresponds to a three-tilt system ($a^-a^-c^+$) [25]. Looking at the theoretical possible sequences of space group changes to be expected with octahedron tilting in perovskite compounds, a transition from *Pbnm* to *Imma* space group is allowed [26]. The *Imma* space group thus seems in good agreement with previous literature and theories on perovskite structure. LSTN25 compound is thus intermediate in terms of symmetry between the two extreme compounds: cubic $SrTiO_3$ and orthorhombic LTN.

Table 1
$La_{0.5}Sr_{0.5}Ti_{0.75}Ni_{0.25}O_{3-\delta}$ prepared in air at 1300 °C for 12 h: structural parameters from Rietveld refinement based on XRD data.

Atom	Site	Occupancy	*x*	*y*	*z*	B_{iso} (Å^2)
La	4e	0.125	0	0.25	0.495(1)	0.30(5)
Sr	4e	0.125	0	0.25	0.495	0.3
Ti	4a	0.1875	0	0	0	0.3
Ni	4a	0.0625	0	0	0	0.3
O(1)	4e	0.25	0	0.25	−0.024(8)	1.5(3)
O(2)	8g	0.5	0.25	0.023(3)	0.25	1.5

Note. Space group *Imma* (74); $a = 5.5285(1)$ Å, $b = 7.8113(2)$ Å, $c = 5.5583(1)$ Å, $V = 240.03(1)$ Å^3, $Z = 4$, $R_{Bragg} = 4.56$, $R_p = 27.0$, $R_{wp} = 31.9$, $R_{exp} = 30.58$, $\chi^2 = 1.09$. From room temperature XRD data recorded in angular range (2θ) 5–120° with a step size of 0.017° (2θ).

The specific surface area of the powder, once treated at 1200 °C for 3 h, was 2.1 m^2 g^{-1}, as determined by the BET method, which is relatively low for the Pechini route. The particle size distribution, determined by laser granulometry, reveals a high size dispersion of agglomerates (d_{50} = 10.9 μm and d_{90} = 62 μm).

On the dilatometric curve of Fig. 2, the early stage of sintering is observed at 1100 °C, and the maximum densification rate is reached at 1350 °C. After cooling, the pellet achieved 95% theoretical density, which was calculated using the refined lattice parameters (d_{th} = 5.85 g cm^{-3}). The same data also allowed the electrode sintering temperature to be determined, a critical parameter during symmetrical cell preparation. The objectives of such a treatment

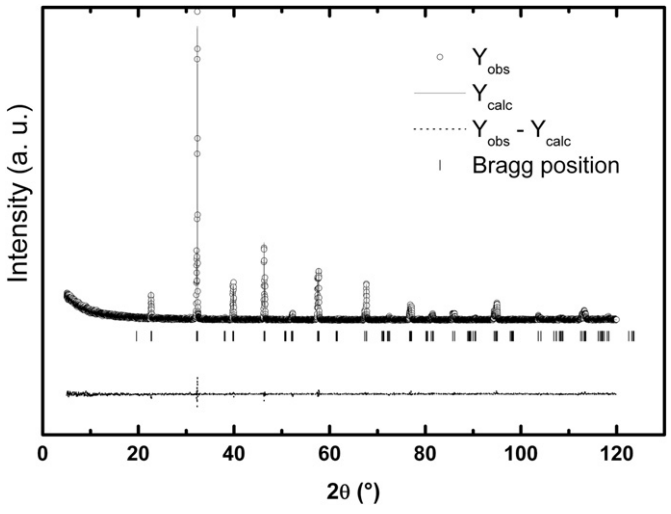

Fig. 1. Rietveld refinement using XRD data of $La_{0.5}Sr_{0.5}Ti_{0.75}Ni_{0.25}O_{3-\delta}$ after synthesis at 1300 °C for 12 h in air.

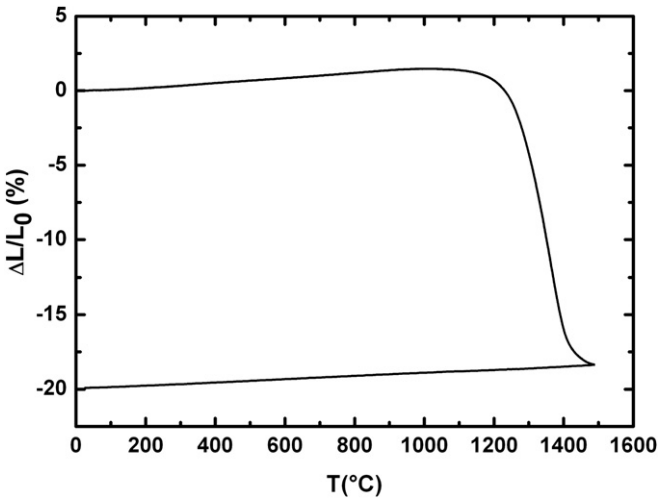

Fig. 2. Dilatometric curve of $La_{0.5}Sr_{0.5}Ti_{0.75}Ni_{0.25}O_3$ measured in air.

are to obtain a homogenous electrode/electrolyte interface without any cracks and to generate a mechanical cohesion without leading to a total electrode densification. From our own experience, a treatment at 1200 °C for 3 h seems therefore reasonable, just following the early stage of sintering. The Thermal Expansion Coefficient (TEC) was also determined from the dilatometric curve using the linear part between 400 and 1000 °C during cooling. With a calculated TEC of 11 $\times$ 10^{-6} K^{-1}, LSTN25 presents a thermo-mechanical behavior close to that of the 8YSZ electrolyte (12 $\times$ 10^{-6} K^{-1}), suggesting a reasonable mechanical compatibility between the two components adjacent in the half cell.

3.2. Study of reduction: exsolution conditions

Thermogravimetric analysis was carried out in Ar/H_2 (98/2) from room temperature to 1500 °C to study the phase stability of LSTN25 (Fig. 3). Significant mass loss starts at 1000 °C and corresponds to oxygen atom departures related to Ni and/or Ti cation reduction. In literature, only *in-situ* reduction (at 800 °C) was proposed as a mechanism for Ni exsolution [17–19]. However, according to the TGA curve, there is no mass loss at 800 °C. Thus, we proposed to pre-reduce LSTN25 at above 1000 °C, trying to obtain exsoluted metallic nickel particles without decomposition of the perovskite structure. Indeed, such treatment beyond 1000 °C is thought to lead to better long-term stability of the SOFC anode, considering that the electrochemical cell has to be used at 800 °C or less. Reduction treatments on the powder were performed in Ar/H_2 (98/2) from room temperature to 1300 °C. To check the possibility of direct Ni exsolution in operating conditions, a reduction treatment was also performed at 800 °C for 48 h.

Corresponding XRD patterns show a clear structural evolution (Fig. 4). LSTN25 compound seems to be stable in diluted H_2 until 1200 °C. The same treatment at higher temperature increases the proportion of Ni^0. The creation of V''_{Ni} induces the segregation of A species and causes the beginning of perovskite structure decomposition with formation of La_2O_3, La_2TiO_5 and Ni^0. Even if no Ni^0 peaks are observed in XRD patterns after reduction at 1200 °C or 800 °C, Ni^0 particles being probably too low in quantity or too small to be detected, TEM observation and energy dispersive X-ray analysis confirm the precipitation of nickel nanoparticles, sized between 5 and 50 nm, after both treatments (Fig. 5). However, nanoparticle density is low, and after several attempts, an estimation of the concentration and average size of Ni^0 nanoparticles through TEM image analysis was found difficult to perform with sufficient accuracy.

Table 2 gives the cell parameters of LSTN25 after the various reduction treatments. Reduction induces an increase of all lattice

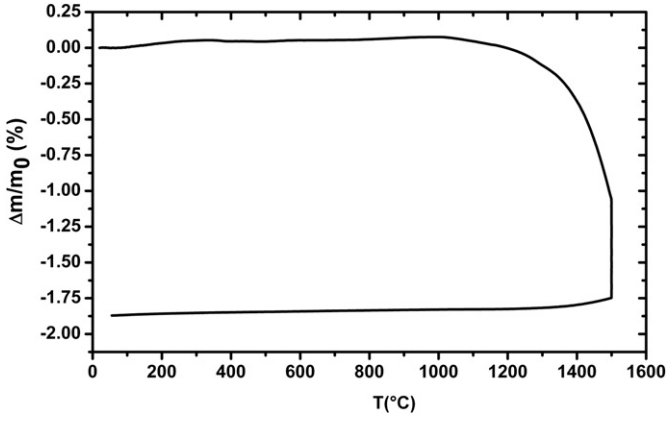

Fig. 3. Thermogravimetric analysis in Ar/H_2 (98/2) of $La_{0.5}Sr_{0.5}Ti_{0.75}Ni_{0.25}O_{3-\delta}$.

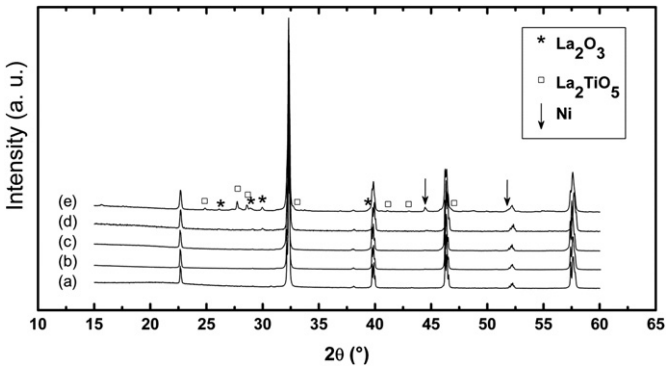

Fig. 4. XRD patterns of LSTN25 samples after reducing treatment at different temperatures: (a) reference corresponding to the sample before reduction; (b) 800 °C for 48 h; (c) 1200 °C for 2 h; (d) 1250 °C for 2 h; (e) 1300 °C for 2 h.

parameters, and the stronger the reduction treatment, the larger the lattice parameter. In detail, reduction at 800 °C for 48 h leads to a relative cell expansion $\Delta V/V$ of 0.24%, confirming that Ni exsolution can occur with an *in situ* reduction. In such mild conditions (at 800 °C with $10^{-20} < pO_2 < 10^{-12}$ atm), the reduction of Ni^{2+} to Ni^0 is thought to be favored with respect to Ti^{4+} to Ti^{3+} reduction, if we compare the thermodynamic equilibrium between NiO/Ni and TiO_2/Ti_4O_7 [11,27]. Nevertheless, the absence of weight loss in the TGA curve is quite intriguing, simultaneously with the Ni^0 particle formation, what means the reduction that is observed at 800 °C must be quite limited.

At higher temperature, greater cell expansion is found, with $\Delta V/V$ close to 0.45%. According to Fig. 3, at $T > 1000$ °C, weight loss is accelerating on the TGA curve but, however, without the possibility to identify two distinct mechanisms, *i.e.*, nickel and titanium reduction. Both Ni^{2+} to Ni^0 and Ti^{4+} to Ti^{3+} reduction may occur at the same time, unless Ti^{4+} is reduced at even higher temperature than 1500 °C. Hence, if only nickel is reduced above 1000 °C in diluted hydrogen, the creation of V''_{Ni} point defects within the perovskite lattice, associated with $V^{\bullet\bullet}_O$ formation, similar to a Schottky defect, can be the only source of cell expansion. This is not surprising in ionic materials, due to the increase in the local counterion–counterion repulsions [28]. In the case of Ti^{4+} being also reduced to Ti^{3+}, which is not possible to confirm at this stage of the study, cell volume increase is in complete agreement with larger Ti ions ($r(Ti^{3+}) = 0.81$ Å and $r(Ti^{4+}) = 0.745$ Å in octahedral coordination [29]).

Overall, cell expansion due to chemical reduction is relatively small and encourages mechanical stability during cell preparation. The exsolution of Ni seems to be possible without major decomposition of the perovskite phase after both kinds of treatments: high-temperature pre-reduction or *in-situ* reduction. It is worth noting that after different thermal cycles, the material is possibly not in the same thermodynamic equilibrium state, with different concentrations of V''_{Ni}, $V^{\bullet\bullet}_O$, or Ti'_{Ti} defects; this means not only different proportions of Ni nanoparticles will be found in both cases, but also different conductivities, related to Ti^{3+} concentration, if titanium cations are partially reduced. This aspect will be addressed in the next section, which gives the conductivity measurements, but it already seems reasonable to affirm that metallic nanoparticles are so dilute and separated in the perovskite substrate that they do not percolate. Thus, Ni nanoparticles do not contribute to electrical conductivity.

3.3. Electrical characterization

Electrical properties of LSTN25 were measured and compared in wet Ar/H_2 (98/2) for samples reduced in the conditions described

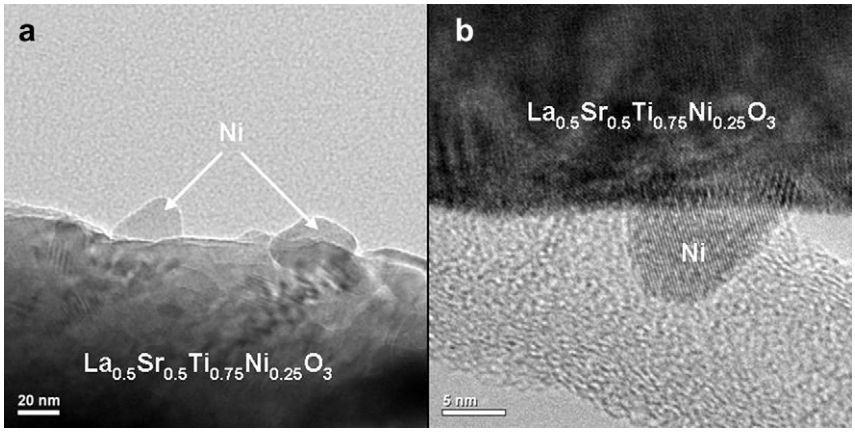

Fig. 5. (a) TEM micrograph of $La_{0.5}Sr_{0.5}Ti_{0.75}Ni_{0.25}O_3$ reduced at 800 °C for 48 h; (b) HRTEM image of a Ni nanoparticle on the LSTN substrate after 2 h pre-reduction at 1200 °C in Ar/H_2 (98/2).

above (*in-situ* or high-temperature reduction). In addition, measurements of as-prepared samples were also carried out in air and Ar/H_2 (98/2). Temperature dependence of electrical conductivity data is plotted in Fig. 6.

In the case of Mixed Ionic and Electronic Conductors (MIEC), the total conductivity measured by the 4-point probe DC method, is the sum of ionic conductivity and electronic conductivity. Depending on the temperature and $p(O_2)$ range, one contribution may be dominant over the other. Table 3 gathers the measurement conditions and the electrical properties.

3.3.1. Electrical behavior of as-prepared samples

For as-prepared samples (■ and ◆ symbols in Fig. 6), the dependence on temperature of electrical conductivity can be fitted by an Arrhenius law:

$$\sigma(T) = \frac{A}{T}\exp\left(-\frac{E_a}{kT}\right) \quad (4)$$

where E_a is the activation energy related to the conduction process, k the Boltzmann constant and A a pre-exponential factor depending on the mobility and concentration of charge carriers. The conductivity in air (■ symbols in Fig. 6) is about ten times higher than that of the same sample measured in Ar/H_2 (98/2) (◆ symbols in Fig. 6). The $p(O_2)$ decrease leads also to an increase of the activation energy (Table 3). This trend was already observed for transition-metal-doped LST compounds such as LSTM or LSTF and was attributed to p-type semi-conductivity. For those materials, conductivity in air is controlled by the mixed valence of the transition metals $Mn^{3+/4+}$ and $Fe^{3+/4+}$ [6,30]. Even if no proof of Ni^{3+} reduction to Ni^{2+} was observed by TGA, the conductivity of LSTN may be controlled by Ni^{3+}/Ni^{2+} in air (p-type).

As a first approximation, LSTN25 corresponds to a solid solution between $SrTi^{+4}O_3$ and $LaTi^{+4}_{0.5}Ni^{+2}_{0.5}O_3$; complete neutralization between $La^{\bullet}_{Sr}$ and Ni''_{Ti} is thus expected in LSTN and oxygen deficiencies δ must approach zero. In air, the charge neutrality condition allows the formation of Ni^{3+} via disproportionation of nickel cations according to the equation:

$$2Ni^{2+} \rightarrow Ni^{+} + Ni^{3+} \quad (5)$$

The proportion of trivalent nickel must be very low (a first reduction step corresponding to Ni^{3+} reduction around 600 °C is not observed by TGA, and additional peaks are absent from XRD patterns). Thus, it is quite logical to observe low conductivity in air because of the low concentration of charge carriers in such conditions. In addition, the rather high activation energy (0.53 eV) indicates that the contribution of ionic conductivity is perhaps not completely negligible in air.

As discussed above, formation of Ti^{3+} does not seem to be favored in LSTN25 in SOFC anodic operating conditions. Moreover, disproportionation of Ni^{2+} (Eq. (5)) is negligible in a reducing atmosphere. Electronic conductivity due to Ti^{4+}/Ti^{3+} and Ni^{3+}/Ni^{2+} mixed valences must be very poor in this material. Thus, conductivity of LSTN25 in Ar/H_2 (98/2) is suggested to be mainly anionic with an activation energy of 0.80 eV.

3.3.2. Influence of reducing treatment

Concerning the sample that was previously reduced at 800 °C for 48 h and measured in SOFC anodic conditions (○ symbols in Fig. 6), the conductivity is nearly one order of magnitude higher than for as-prepared samples measured in reducing conditions (at the same level as as-prepared samples measured in air); the main difference is the higher slope with respect to previous samples. The

Table 2
Unit cell parameters of $La_{0.5}Sr_{0.5}Ti_{0.75}Ni_{0.25}O_3$ after various thermal treatments.

Firing conditions	Lattice parameters	Secondary phase
1300 °C/12 h in air	a = 5.5285(1) Å, b = 7.8113(2) Å, c = 5.5583(1) Å, V_0 = 240.03(1) Å^3	None
1300 °C/12 h in air then 800 °C/48 h in Ar/H_2 (98/2)	a = 5.5328(2) Å, b = 7.8183(3) Å, c = 5.5623(2) Å, V = 240.61(2) Å^3, $\Delta V/V_0$ = +0.24%	None
1300 °C/12 h in air then 1200 °C/2 h in Ar/H_2 (98/2)	a = 5.5362(2) Å, b = 7.8231(3) Å, c = 5.5671(2) Å, V = 241.11(1) Å^3, $\Delta V/V_0$ = +0.45%	None
1300 °C/12 h in air then 1250 °C/2 h in Ar/H_2 (98/2)	a = 5.5366(6) Å, b = 7.8232(8) Å, c = 5.5676(5) Å, V = 241.15(4) Å^3, $\Delta V/V_0$ = +0.47%	0.48 wt% Ni^0, 0.34 wt% La_2O_3
1300 °C/12 h in air then 1300 °C/2 h in Ar/H_2 (98/2)	a = 5.5374(4) Å, b = 7.8242(6) Å, c = 5.5650(4) Å, V = 241.10(3) Å^3, $\Delta V/V_0$ = +0.45%	2.14 wt% Ni^0, 0.47 wt% La_2O_3, 6.67 wt% La_2TiO_5

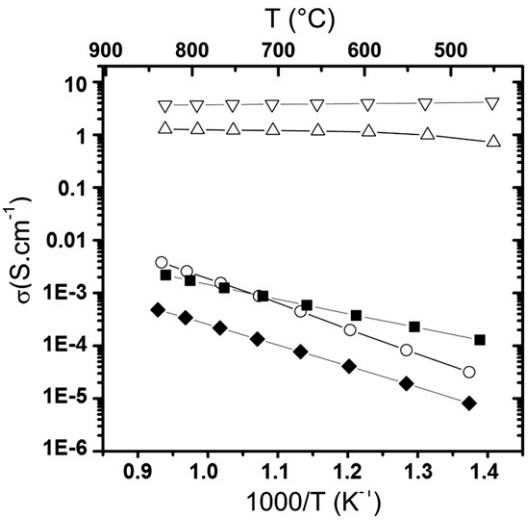

Fig. 6. Conductivity *vs.* reciprocal temperature for LSTN25: as-prepared sample measured (■) in air and (◆) in Ar/H_2 (98/2); sample measured in humidified Ar/H_2 (98/2) ($pH_2O = 0.025$ atm) after reduction (▽) in Ar/H_2 (98/2) at 1200 °C for 2 h, (△) after reduction at 1200 °C for 2 h followed by an oxidation at 800 °C for 5 h in air and (○) after reduction at 800 °C for 48 h.

value of activation energy, nearly 1 eV, is quite typical of ionic conductivity. Following the former discussion, reduction of Ti^{4+} to Ti^{3+} is probably not favored at 800 °C. The long reduction step at 800 °C should be responsible for a significant increase in the concentration of oxygen vacancies, associated with exsolution of Ni and B-site deficiencies. As a consequence of a longer reduction treatment, the LSTN25 sample that has been pre-reduced at 800 °C may have a higher concentration of oxygen vacancies than an as-prepared sample, resulting in a higher ionic conductivity.

Concerning the sample that was pre-reduced at 1200 °C for 2 h (▽ symbols in Fig. 6), conductivity is greatly improved (up to a factor of 10^3 at 800 °C), and surprisingly, the conductivity slightly increases as temperature decreases. This behavior, characteristic of metals, can be attributed to the formation of Ti^{3+} ($3d^1$) and has already been observed for La- or Y-substituted $SrTiO_3$ [2,10,31–35]. Indeed, LST and YST compounds are known to show a strong improvement in electrical properties after sintering in a reducing atmosphere due to the reduction of Ti^{4+} to Ti^{3+} according to the following reaction, using Kröger–Vink notation [2]:

$$2Ti_{Ti}^{X} + O_{O}^{X} + H_2 \rightarrow 2Ti_{Ti}^{/} + V_{O}^{\bullet\bullet} + H_2O \quad (6)$$

In donor-substituted $SrTiO_3$, electrical conductivity is essentially controlled by the concentration of the electronic defect $Ti_{Ti}^{/}$, depending on the degree of La^{3+} or Y^{3+} substitution and the thermodynamic equilibrium state. Any change of pO_2 or temperature leads to a new equilibrium state. The higher the temperature used for the reducing treatment, the higher the electronic defect concentration.

With $\sigma = 2.3$ S cm^{-1} at 800 °C, LSTN25 pre-reduced at high temperature reaches the conductivity necessary for an SOFC functional anode layer [36]. However, this high-temperature pre-reduction treatment is interesting only if the sample does not re-equilibrate thermodynamically in operating conditions. In donor doped-$SrTiO_3$ or $BaTiO_3$, it was shown that after a higher-temperature reduction, compounds treated at 800 °C in a reducing atmosphere cannot return to thermodynamic equilibrium, due to poor ion diffusion kinetics, and they retain a high conductivity [31]. In addition, the phase obtained after the high temperature pre-reduction must also resist the redox cycles inherent to SOC operating conditions. In this context, conductivity of the pre-reduced sample was measured after one redox cycle (at 800 °C for 5 h in air) to answer this question of stability or metastability (△ symbols in Fig. 6). After such treatment, a conductivity decrease was observed, though by less than a factor of two, that was judged not extremely detrimental for the application. In fact, a small degradation of conductivity after redox cycling was also observed for other substituted titanates [1,2,10,33,34]. Hashimoto *et al.* showed that, after strong reduction, conductivity of Nb-doped $SrTiO_3$ in a reducing atmosphere was not affected by redox cycles, whereas that of LST dropped upon exposure to air and never recovered after re-reduction [34]. They explain these behaviors by differences in oxygen diffusivity after strong reduction. Fu *et al.* reported that a stable value is reached for YST after several redox cycles, suggesting that a new equilibrium state (with lower electrical conductivity than in the initial state) is obtained [10]. In our study, although a small decrease of LSTN conductivity is observed after one redox cycle, the order of magnitude of conductivity is maintained, far from that of the non-reduced sample (◆ symbols in Fig. 6). This result is very promising for the use of a pre-reduced phase as a hydrogen electrode.

Overall, conductivity behavior, long-term stability and redox stability of the pre-reduced phase must be studied further to be discussed in terms of defect chemistry. Indeed, exsolution of Ni is a surface process and may induce disorder and a composition gradient in grains, especially if thermodynamic equilibrium is not completely reached. In addition, the structure and properties of substituted $SrTiO_3$ perovskites are known to be very dependent on preparation conditions [32]. They can accommodate extended lamellar defects and over-stoichiometric oxygen (additional oxygen with respect to the stoichiometric composition) to ensure charge compensation depending on $p(O_2)$. Moreover, it was shown that grain boundaries influence the conduction properties [34,35]. All these phenomena may play a significant role in the stability and redox behavior of LSTN compounds and require deeper studies using additional techniques like electronic diffraction for extended defect identification, magnetic characterization using Electron Paramagnetic Resonance (EPR) or Superconducting Quantum Interference Device (SQUID) to evidence the presence of Ti^{3+}.

Table 3
Activation energy and total conductivity at 800 °C of LSTN25 samples after different pre-treatments and measured in several atmospheres.

Atmosphere	Pre-treatment	Activation energy (eV)	σ_{corr} (S cm^{-1}) at 800 °C
Air	None	0.53 (300–800 °C)	2.2×10^{-3}
Ar/H_2 (98/2)	None	0.80 (300–800 °C)	4.9×10^{-4}
Ar/H_2 (98/2), $pH_2O = 0.025$ atm	2 h at 1200 °C in Ar/H_2 (98/2)	~0	2.3
	2 h at 1200 °C in Ar/H_2 (98/2) then 5 h at 800 °C in air	0.05 (500–800 °C)	1.4
	48 h at 800 °C in Ar/H_2 (98/2)	0.94 (450–800 °C)	3.8×10^{-3}

3.4. Electrochemical characterization

Symmetrical cells were prepared to evaluate the electrochemical performance of LSTN25 as a new hydrogen electrode material. Fig. 7 presents the Nyquist diagram obtained at 800 °C in H_2/H_2O (97/3) for the symmetrical cell pre-reduced at 1200 °C for 2 h and for the symmetrical cell pre-reduced at 1200 °C for 2 h and then re-oxidized at 1100 °C for 3 h (conventional sintering

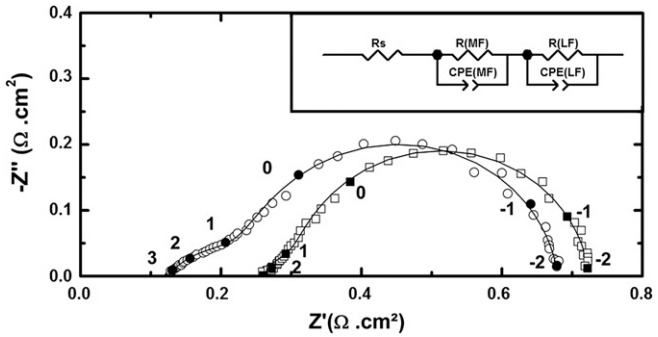

Fig. 7. Electrochemical performance of symmetrical cells with 8YSZ//YDC (5 μm)/LSTN25(15 μm)/Ni(10 μm) architecture. (○) Pre-reduction at 1200 °C for 2 h and (□) pre-reduction at 1200 °C for 2 h then re-oxidation at 1100 °C for 3 h. Closed symbols and numbers beside them indicate the order of magnitude of frequency (10^{-2} to 10^{3} Hz). Solid lines are the fitted data with the equivalent circuit shown in the inset.

conditions for a (La,Sr)MnO_3 air electrode). Impedance spectra were fitted using the equivalent circuit $R_s(R\text{-CPE})_1(R\text{-CPE})_2$ (shown in the inset of Fig. 7). R_s is the ohmic resistance mainly ascribed to the electrolyte, R_i is an ohmic resistance, and CPE_i the constant phase element of the limiting phenomenon *i*. The series connections of $(R\text{-CPE})_1$ and $(R\text{-CPE})_2$ correspond to the two observed arcs at medium (MF) and low frequencies (LF), respectively. The fit obtained using this model was in good agreement with the experimental data. Resistance values, relaxation frequency f_i and specific capacity C_i calculated based on the refined lattice parameters are listed in Table 4, where polarization resistance (R_p) is defined as $R_1 + R_2$.

The limiting steps usually considered for the H_2 oxidation reaction are [37,38]:

- dissociative H_2 adsorption and diffusion on the Ni surface or H_2 gas diffusion inside the porous electrode, corresponding to low frequency (LF) and medium frequency (MF) contributions,
- charge transfer reaction at the electrode and electrolyte interface corresponding to a high frequency (HF) contribution.

For an LSTN-based electrode, the major contribution is at low frequency and may be reduced by playing on the microstructure of the electrode in order to increase porosity. No HF contribution is observed, indicating good electronic and/or ionic transfer through the electrolyte//electrode interface. This is generally the case for an electrode with a thin doped ceria interlayer. However, this YDC interlayer complicates the attribution of contributions to physical phenomena [38].

Polarization resistance measured on the LSTN25-based cell reaches about 0.55 Ω cm^2 at 800 °C in wet H_2 (with 3% H_2O). This value is higher than for conventional Ni/YSZ cermets ($R_p < 0.3$ Ω cm^2 at 800 °C) [39] or an optimized YST/YSZ composite electrode impregnated with 5 vol% Ni ($R_p = 0.21$ Ω cm^2 at 800 °C) [10]. However, measurements were performed after only 1 h of stabilization at 800 °C and during this time, polarization resistance continuously decreased, probably due to further Ni exsolution or Ti reduction. Longer stabilization may thus give better results, and, as discussed above, optimizing microstructure could still improve those preliminary results. Finally, whereas conventional Ni-based cermets are known to suffer re-oxidation [40], thermal treatment at a typical temperature for the sintering of (La,Sr)MnO_3 air electrode material (1100 °C for 3 h) does not affect performance of the LSTN25 material. On the contrary, polarization resistance stays as low as 0.46 Ω cm^2 at 800 °C, even if an increase of ohmic resistance is observed due to the re-oxidation of LSTN25 (see the discussion above concerning the influence on the conductivity of a thermal treatment in air) and/or possible delamination of the Ni-collecting layer. This result is encouraging for the future preparation and study of complete LSTN-based cells.

Table 4
Specific resistance values determined by fitting of the electrochemical impedance spectra shown in Fig. 7.

Sample	R_s (Ω cm^2)	R_p (Ω cm^2)	MF contribution	LF contribution
LSTN25 pre-reduced 2 h at 1200 °C	0.12	0.55	$R = 0.12$ Ω cm^2 $f = 17.8$ Hz $C = 30$ mF cm^{-2}	$R = 0.43$ Ω cm^2 $f = 0.4$ Hz $C = 0.5$ F cm^{-2}
LSTN25 pre-reduced 2 h at 1200 °C and reoxidized 3 h at 1100 °C	0.26	0.46	$R = 0.06$ Ω cm^2 $f = 10.9$ Hz $C = 120$ mF cm^{-2}	$R = 0.40$ Ω cm^2 $f = 0.4$ Hz $C = 0.5$ F cm^{-2}

4. Conclusion

Perovskite oxide $La_{0.5}Sr_{0.5}Ti_{0.75}Ni_{0.25}O_{3-\delta}$ was successfully synthesized and its behavior under reduction characterized. TEM study evidenced the partial exsolution of Ni above 800 °C in diluted H_2. After a high-temperature reduction (1200 °C), LSTN25 exhibits a metallic behavior in a reducing atmosphere, and its conductivity increased by up to a factor of 1000 at 800 °C, reaching the specifications for a functional hydrogen electrode. Such enhancement was attributed to the increase in Ti^{3+} concentration. Conductivity remains high after a redox cycle. Overall, this behavior must be further studied to better understand this phenomenon in terms of defect chemistry. This result raised the issue of long-term stability of the pre-reduced phase and, especially how competition between Ti reduction and Ni exsolution is reflected through the mechanism of charge compensation.

Electrochemical performance is promising, with a polarization resistance of 0.55 Ω cm^2 at 800 °C under H_2/H_2O (97/3), which was even better after a sintering step in air (simulating air electrode sintering). Finally, this work shows the interest of further study of the (La,Sr)(Ti,Ni)O_3 series as new hydrogen electrode materials for SOC.

Acknowledgments

The authors thank E. Gautron from IMN for the TEM micrographs and Dr. M. Caldes for useful discussions.

References

[1] S. Hui, A. Petric, J. Electrochem. Soc. 22 (2002) 1673–1681.
[2] O.A. Marina, N.L. Canfield, J.W. Stevenson, Solid State Ionics 149 (2002) 21–28.
[3] J. Sfeir, P.A. Buffat, P. Möckli, N. Xanthopoulos, R. Vasquez, H.J. Mathieu, J. Van Herle, K.R. Thampi, J. Catal. 202 (2001) 229–244.
[4] R. Mukundan, E.L. Brosha, F.H. Garzon, Electrochem. Solid-State Lett. 7 (2004) A5–A7.
[5] J.C. Ruiz-Morales, J. Canales-Vázquez, C. Savaniu, D. Marrero-López, W. Zhou, J.T.S. Irvine, Nature 439 (2006) 568–571.
[6] Q.X. Fu, F. Tietz, D. Stöver, J. Electrochem. Soc. 153 (2006) D74–D83.
[7] J. Liu, B.D. Madsen, A. Ji, S.A. Barnett, Electrochem. Solid-State Lett. 5 (2002) A122–A124.
[8] B.D. Madsen, S.A. Barnett, J. Electrochem. Soc. 154 (2007) B501–B507.
[9] M.D. Gross, J.M. Vohs, R.J. Gorte, J. Mater. Chem. 17 (2007) 3071–3077. and references therein.
[10] Q. Fu, F. Tietz, D. Sebold, S. Tao, J.T.S. Irvine, J. Power Sourced 171 (2007) 663–669.
[11] K. Takehira, Catal. Surv. Jpn. 6 (2002) 19–32.
[12] C.H. Bartholomew, Catal. Rev. Sci. Eng. 24 (1982) 67–112.
[13] T. Hayakawa, S. Suzuki, J. Nakamura, T. Uchijima, S. Hamakawa, K. Suzuki, T. Shishido, K. Takehira, Appl. Catal., A: Gen. 183 (1999) 273–285.
[14] J. Guo, H. Lou, Y. Zhu, X. Zheng, Mater. Lett. 57 (2003) 4450–4455.

[15] G.S. Gallego, F. Mondragón, J. Barrault, J.-M. Tatibouët, C. Batiot-Dupeyrat, Appl. Catal,. A: Gen. 311 (2006) 164–171.
[16] J.R. Mawdsley, T.R. Krause, Appl. Catal., A: Gen. 334 (2008) 311–320.
[17] B.D. Madsen, W. Kobsiriphat, Y. Wang, L.D. Marks, S.A. Barnett, ECS Trans. 7 (2007) 1339–1348.
[18] W. Kobsiriphat, B.D. Madsen, Y. Wang, M. Shah, L.D. Marks, S.A. Barnett, J. Electrochem. Soc. 157 (2010) B279–B284.
[19] T. Jardiel, M.T. Caldes, F. Moser, J. Hamon, G. Gauthier, O. Joubert, Solid State Ionics 181 (2010) 894–901.
[20] T. Delahaye, G. Gauthier, Titanates de structure pérovskite ou dérivée et ses applications, French Patent N° 08 02032, April 14th, 2008.
[21] Juan Rodriguez-Carvajal, Thierry Roisnel, New Windows 95/NT applications for diffraction commission for powder diffraction, IUCr Newsletter N°20 (May–August) (Summer 1998).
[22] A. Boultif, D. Louer, J. Appl. Crystalogr 24 (1991) 987–993.
[23] J. Lougier, B. Bochu, Checkcell: Graphical Powder Diffraction Indexing Cell and Space Group Assignment Software. Available from: http://www.inpg.fr/LMGP.
[24] E. Rodriguez, I. Alvarez, M.L. Lopez, M.L. Veiga, C. Pico, J. Solid State Chem. 148 (1999) 479–486.
[25] P.M. Woodward, Acta Crystallogr. B53 (1997) 32–66.
[26] R.H. Mitchell, Perovskites Modern and Ancient, Almaz Press, Thunder Bay, Ontario, 2002.
[27] D.C. Lynch, D.E. Bullard, Metall. Mater. Trans. B 28 (1997) 447–453.
[28] A. Gaber, H. Zillgen, P. Ehrhart, P. Partyaka, R.S. Averback, J. Appl. Phys. 82 (11) (1997) 5348;
J. Corish, P.W.M. Jacobs, Surface and Defects Properties of Solids, In: Chemical Society Specialist Periodical Reports, vol. 2, The Chemical Society, London, 1973.
[29] R.D. Shannon, Acta Crystallogr. A32 (1976) 751–767.
[30] D.P. Fagg, V.V. Kharton, J.R. Frade, A.A.L. Ferreira, Solid State Ionics 156 (2003) 45–57.
[31] Q. Fu, S. Mi, E. Wessel, F. Tietz, J. Eur. Ceram. Soc. 28 (2008) 811–820.
[32] S. Hashimoto, L. Kindermann, F. Poulsen, M. Mogensen, J. Alloys Compd. 397 (2005) 245–249.
[33] S. Hashimoto, L. Kindermann, P. Larsen, F. Poulsen, M. Mogensen, J. Electroceram. 16 (2006) 103–107.
[34] S. Hashimoto, F. Poulsen, M. Mogensen, J. Alloys Compd. 439 (2007) 232–236.
[35] R. Moos, K.H. Härdtl, J. Appl. Phys. 80 (1996) 393–400.
[36] A. Atkinson, S. Barnett, R.J. Gorte, J.T.S. Irvine, A.J. McEvoy, M. Mogensen, S.C. Singhal, J. Vohs, Nat. Mater. 3 (2004) 17–27.
[37] S. Jiang, X. Chen, S. Chan, J. Kwok, K. Khor, Solid State Ionics 177 (2006) 149–157.
[38] S. Tao, J.T.S. Irvine, J. Electrochem. Soc. 151 (2004) A252–A259.
[39] S. Primdahl, Ph.D. Thesis, University of Twente, Twente, The Netherlands, 1999.
[40] M. Pihlatie, T. Ramos, A. Kaiser, J. Power Sources 193 (2009) 322–330.